A DEM based tool for the safety analysis of masonry gravity dams

Eduardo M. Bretas[1], José V. Lemos[2], Paulo B. Lourenço[3]

1. Eduardo M. Bretas (corresponding author): Postdoctoral Researcher, National Laboratory for Civil Engineering, Av. do Brasil, 101, 1700-066, Lisbon, Portugal, E-mail: ebretas@lnec.pt, Phone: (351) 218 443 000, Fax: (351) 218 443 026

2. José V. Lemos: Researcher, National Laboratory for Civil Engineering, E-mail: vlemos@lnec.pt

3. Paulo B. Lourenço: Professor, Department of Civil Engineering, University of Minho, E-mail: pbl@civil.uminho.pt

Abstract: A numerical model for analysis of masonry gravity dams based on the discrete element method is presented. The dam and the rock foundation are represented as block assemblies, using elementary 3- and 4-node blocks. Complex block shapes are obtained by assembling the elementary blocks into macroblocks, allowing the model to be applied in various situations ranging from equivalent continuum to fully discontinuum analysis. A contact formulation was developed, which represents the interaction between macroblocks in terms of contacts established between elementary blocks, based on an accurate edge-edge approach. The main numerical aspects of the model are described, addressing in particular the contact creation and update procedures, and the numerical devices that support an efficient explicit solution algorithm. An application to the safety evaluation of an existing masonry dam is discussed, including stress analysis in the structure, and the assessment of sliding failure mechanisms, involving different paths in the vicinity of the dam-rock interface.

Keywords: Masonry dams, discrete elements, stress analysis, failure mechanisms

1. Introduction

Structural analysis must use appropriate methods to achieve its final purposes. These methods should be capable of (i) modelling the geometrical and physical characteristics of the structure, in particular the discontinuities and joints, (ii) modelling the loads in an integrated manner, taking into account the interaction between the relevant phenomena involved, and (iii) evaluating the non-linear behaviour, particularly allowing the definition of failure mechanisms.

Masonry gravity dams should be understood as a system composed of the dam itself, the reservoir, and the rock mass foundation. The dam and the rock mass are heterogeneous and discontinuous media. The dam-rock interface is also a discontinuity which requires particular attention. The discontinuity surfaces control the behaviour of masonry dams, because they are weakness planes that determine the main mechanisms of failure. In addition, dams are subject to a wide variety of loads requiring an integrated approach since they are often correlated. These particular features make the majority of the available numerical tools, both commercial and scientific, not entirely suitable for modelling masonry gravity dams. In this context, the development of new analysis tools is required. Here, a tailored numerical implementation of the Discrete Element Method (DEM) for static, dynamic and hydromechanical analysis of masonry gravity dams is described.

The Discrete Element Method was initially proposed as an alternative to the Finite Element Method (FEM) to address Rock Mechanics problems [1]. DEM was based on the representation of the discontinuous media as an assembly of blocks in mechanical interaction, thus differing from the standard FEM approach based on joint elements [2,

3]. These numerical approaches have also been widely applied to masonry structures [e.g. 4]. The 2D code UDEC [5], which evolved from Cundall's pioneering work, has been used in several studies involving concrete dam foundations, mostly intending to assess failure mechanisms through the rock mass [e.g. 6, 7, 8]. Tatone et al. [9] performed a DEM analysis of sliding on the dam-rock interface, considering a detailed representation of the irregular geometry of this surface and the ensuing stress concentrations.

Discrete Element Method codes usually represent deformable blocks by discretizing them into an internal mesh of triangular uniform strain elements (e.g., [5]). The designation "discrete finite-element method" [10, 17] is often applied to codes that allow the breakage of the block elements to simulate progressive failure processes. The model presented in this paper is based on DEM and was devised with three main requirements, implemented in a novel software tool fully developed by the authors. Firstly, it is intended to model in an integrated manner both the masonry dam and the rock foundation as components of a blocky system. Secondly, the software tool should provide a practical means to address both equivalent continuum and blocky models, using the same mesh. Finally, the tool needs to include all the features required in dam engineering analysis, such as water flow and pressures in the joints, reinforcement elements, such as passive or active anchors, and the means to apply the loads involved in static and seismic analysis. All these components interact through a compatible data structure. Therefore, the present model combines the standard DEM capabilities in a more general framework, which allows combining rigid and deformable blocks, continuum meshes and discrete components, as required by the application. Moreover, a non-traditional contact formulation is adopted, based on edge-edge interaction, which provides a more accurate stress representation in the interface. The new code shares

with DEM the capability to simulate fracturing of a continuum into blocks through predefined paths, but adopts a representation of contact based on the joint stiffnesses and constitutive laws appropriate for masonry and rock, not following, for example, Munjiza's formulation of contact force potentials [17]. The aspects related to the mechanical calculation will be discussed in detail in the following sections, and an example of application to the safety assessment of a masonry dam in operation will be presented. The hydraulic analysis of the dam and rock foundation, also incorporated in the newly developed analysis tool, was described in a different paper [11].

2. Model discretization and contacts

The numerical tool is intended to model systems composed of a masonry dam and its rock foundation, as shown schematically in Figure 1. Two-dimensional analysis is conservatively assumed for these structures, following common design practices and dam safety codes [e.g. 12, 13, 14], for practical reasons: historically, masonry dams were designed as gravity dams; arching effects cannot be guaranteed; and, the computational model is simpler to understand. The fundamental element of discretization of the structure is the block with three or four edges, which may be rigid or deformable, and can be used simultaneously in the same model. The structure, characteristics and objectives of the analysis should dictate the choice of blocks. In terms of performance, the calculation is faster for the rigid blocks because the equation of motion is established only in the centroid of the element, thus reducing the degrees of freedom of the model. The computational advantage of rigid blocks is only relevant in explicit dynamic analysis, since static solutions are usually very fast to obtain. In dam engineering, stress analysis in the structure and foundation is usually required, so

deformable blocks are preferred. In case of deformable blocks, each block is assumed here as an isoparametric linear finite element with full Gauss integration.

Blocks of general shapes may be created by assembling the 3 and 4 node blocks into macroblocks. This is an important feature to model discontinuous media, such as masonry dams and rock mass foundations. In this way, it is possible to adopt an equivalent continuum representation of the whole system, or part of the system, in which each block is just an element of the FEM mesh.

A macroblock is a combination of blocks, forming a continuous mesh, in which the vertices are coincident. Between the blocks of the same macroblock, relative movement is not permitted, so there are no contact forces. The macroblock is similar to a finite element (FE) mesh but with an explicit solution because the assemblage of a global stiffness matrix does not take place. Figure 2a shows a discontinuous model composed by two individual blocks. A similar model, but continuous, composed by one macroblock, is presented in Figure 2b. Another continuum model, similar to a FE mesh is showed in Figure 2c. A hybrid model, composed by two macroblocks, is presented in Figure 2d, with an explicit joint considered between the two macroblocks.

The macroblock has a data structure containing a list of blocks and a list of macronodes, with a master node and several slave nodes. The macronode has the same degrees of freedom of any individual node, and all numerical operations can focus only on the master node. During the calculation cycle, all forces from the slave nodes must be concentrated in the master node, and after calculation of new coordinates, slave nodes are updated from the respective master node. Despite these procedures, the use of macroblocks has the advantage of reducing the number of contacts and the number of

degrees of freedom. The same model may have several macroblocks and each macroblock can have blocks with different materials.

2.1. Face-to-face contact formulation

The mechanical interaction between two blocks is defined as a numerical contact. In the newly developed software, the fundamental contact type is face-to-face (in the 2D case, it means edge-to-edge) [10, 17], which can degenerate into contacts of type vertex-to-face. The use of face-to-face contact is not usual in DEM and allows different stress integration schemes to obtain contact forces. It allows a linear distribution of stress and a proper application of the joint constitutive model. Thus, the distribution of the contact forces is statically consistent with the diagrams and the bending stiffness is correct. In a face-to-face contact, the face of one block can be fully in contact with the face of another block, a contact face-to-face type 1 (FF_1), or the face of a block is partially in contact with the face of the other block, contact type 2 (FF_2) (Figure 3).

The process of detecting and updating the contact has three stages. The first stage corresponds to the detection, when the contact is established and made active. In the second stage the contact is updated according to the relative movement of the blocks during the analysis. The third stage is to check the validity of the contact geometric assumptions that existed when it was created. The analyses can be performed for the scenarios of "fixed connectivity" or "variable connectivity". In the "fixed connectivity" assumption, the coordinates of the blocks and the orientation of the edges on which the contacts are established are updated at every step. However, the contacts are established only at the beginning of the mechanical calculation and will remain throughout the analysis with the initial type. In the case of "variable connectivity", the coordinates of

the vertices and the orientation of the edges in contact are updated at each calculation cycle. In addition, when the cumulative displacement exceeds a given tolerance, three additional operations are triggered, which include (i) updating the geometry of the blocks, (ii) verifying if the existing contacts hold and (iii) searching for new contacts. The verification includes confirmation of existing contacts and their typology. In this phase a contact can be maintained, eliminated or reclassified. The "variable connectivity" is the general case and is applied in the present paper. The "fixed connectivity" is preferable when large displacements are not expected, or when large displacements have no influence on the failure mechanisms under investigation, because it is faster and more robust.

2.2. Detection and activation of contacts

The detection of contacts involves a set of conventional operations, but the number of blocks in the model can make the process unfeasible. In order to avoid this problem, it is necessary to adopt a phased strategy for detection. The scheme adopted is based on the solution proposed by Cundall [15], although other alternatives are possible. Examples of alternative solutions are given in Williams and O'Connor [16], for concave and convex blocks, and Munjiza [17], using more complex data structures.

The search and detection of contacts is a process with three successive steps. In a first step, which focuses on the entire model, a cell mesh is created. This mesh covers the total area of blocks, increased to account for the expected displacement of the blocks. The blocks are mapped within the cells according to their position and the number of cells should be selected so that they are not too few (with many blocks inside) or too many (with increasing times to scan the contacts). In the second step, the analysis of

proximity at each cell is checked. If two blocks are in the same cell with an overlap between the respective envelopes, a "potential" contact is created. The advantage of this procedure is that the overlap of the block envelopes is only checked between blocks that share a cell and not among all the blocks. In the third step the "potential" contacts are analysed. For this purpose it is necessary to extend the criteria for classification of contacts. The contact type FF_1 can be further classified as type 21 wherein the block 2 is fully supported on block 1, and as type 12, in which the block 1 is fully supported on block 2 (Figure 3). The contact type FF_2 can be classified as type i, when the starting point of each edge is in contact with the opposite edge, and can be classified as type f, when the end point of each edge is in contact with the opposite edge (Figure 3).

The definition of different types and subtypes is needed since the numerical implementation of the face-to-face contact involves two sub-contacts (sct_1 e sct_2), whose origin points are located at the corners of the blocks. Thus, in the contact type FF_1 only one block is the carrier of the two sub-contacts, whereby the influence length of the contact ($L_{i,1} + L_{i,2}$) is the length of this edge. In the contact type FF_2, each block has a sub-contact, and to determine the influence length of the contact it is necessary to take into account the relative position of the two blocks (Figure 4).

The criterion for the activation of contacts is based on the opening of the sub-contacts sct_1 and sct_2. If the opening of both sub-contacts is equal to or less than a tolerance (*tol*), the contact becomes active and numerical sub-contacts are set depending on the type of contact, FF_1 or FF_2. Activation of the contact and its classification depend on a set of geometric parameters determined in relation to each pair of blocks. Based on these parameters a set of prerequisites for the establishment of contact, according to the type, are defined. For each sub-contact, the direction of the opposite edge defines the local

normal and shear components. Thus, in contacts type FF_1-21, the edge of the block 1 controls the orientation of sub-contacts. In contacts type FF_1-12, the edge of the block 2 determines the orientation of the sub-contacts. Finally, in contacts type FF_2-i and FF_2-f, both edges are important because each sub-contact will act on one edge.

The essential data structure for the sub-contact definition includes the source edge, the destination edge, the vertex from which the sub-contact is created, the sub-contact opening (u_n), the influence length of the sub-contact (L_i) and, finally, the distribution length (L_d) of the sub-contact, i.e. the distance between the installation vertex, projected on the opposite edge, to the starting point of this edge. The distribution length is needed since the distribution of the contact force by the vertices of the opposite edge will be based on this parameter. Figure 4 shows the data structure for the contact type FF_1-21 and FF_2-i.

2.3. Contact updating

The updating of the contact is made in each cycle, both in the case of "fixed connectivity" as in the case of "variable connectivity". This update is based on the relative movement of the blocks. Initially the orientation of the edges for which sub-contacts apply is updated, without updating the length of the edges. The velocity of the vertex where the sub-contact is installed is known, but the velocity of the equivalent point, projected on the edge where the sub-contact acts, needs to be determined. The variation of the sub-contact separation is incremental and depends on the time step,

$$\Delta u_x = v_{rel,x}\Delta t \tag{1}$$

$$\Delta u_y = v_{rel,y}\Delta t \tag{2}$$

where Δu_x and Δu_y are the incremental variations of the contact opening, *x* and *y* components; $v_{rel,x}$, $v_{rel,y}$ are the relative velocities of the points that define the sub-contact, *x* and *y* components; and Δt is the time step.

The normal and the tangential components are determined according to the orientation of the edge where the sub-contact acts,

$$\Delta u_n = \Delta u_x n_x + \Delta u_y n_y \tag{3}$$

$$\Delta u_s = \Delta u_x s_1 + \Delta u_y s_2 \tag{4}$$

where Δu_n and Δu_s are the incremental variations of the opening and the tangential length of the contact; (n_x, n_y) are the normal direction definition; and (s_x, s_y) is the tangential direction definition. This approach keeps the continuity in case of contact transition from face-to-face to vertex-to-face as detailed in the next section.

2.4. Contact verification

The contact verification involves three separate stages and includes the (i) update of the envelope of the blocks and the orientation of the edges, (ii) verification of the active contacts and (iii) detection of new contacts. The update of the edges orientation covers all blocks in the model and occurs simultaneously with the update of the length of the edges.

The verification of active contacts can trigger the maintenance, reclassification or elimination of contacts. The decision criteria are based on a procedure similar to that used to detect the contact and the establishment of initial sub-contacts. If the existing contact meets the criteria required to maintain the current classification only the

parameters L_i (influence length) and L_d (distribution length) are updated. There is the possibility that the contact exists but does not meet the criteria required to maintain the same classification. The allowed reclassifications, depending on the current classification, are indicated in Figure 5a. For example, the contact type FF_1-12 may be reclassified as FF_2-i or FF_2-f, but the direct transition to type FF_1-21 is not possible. The reclassification process involves the determination of new sub-contacts (sct_1 e sct_2), which shall receive the parameters u_n e u_s of the existing sub-contacts (sct_1' e sct_2'). According to Figure 5a, in the transitions represented by horizontal arrows the new sub-contact sct_1 receives the parameters u_n and u_s from the existing sub-contact sct_1' and the new sub-contact sct_2 receives the parameters u_n and u_s from the old sub-contact sct_2'. In the reclassification represented by the vertical arrows the change occurs in the order of sub-contacts, so sub-contact sct_1 receives the parameters from sub-contact sct_2', while sub-contact sct_2 receives the parameters from sub-contact sct_1'.

The verification is not performed for all contacts, but only if one of the blocks involved in the contact is "upgradeable", which is the default state. This status can be changed to reduce the number of blocks involved in the contact computation in order to improve the numerical performance. These criteria are adopted also for the detection of new contacts.

It is noted that only contacts face-to-face are considered above. The reason is that all contacts, created in the first iteration, are assumed to be of the type face-to-face. It is possible that the contact face-to-face degenerates to a vertex-to-face contact type, if one sub-contact opening is greater than the tolerance, while the other sub-contact opening remains lower than the tolerance. Figure 5b shows an example of a contact of the type FF_1-21. If the opening $u_{n,2}$ is greater than the tolerance but the opening $u_{n,1}$ is lower than the tolerance, or the reverse, the contact can degenerate to the type vertex-to-face.

2.5. Determination of the contact forces

The contact forces are calculated from the integration of the stress diagram established in the contact. The stresses are determined based on the normal and tangential movement of the sub-contacts, updated at each iteration, and the properties of the joint material, in particular the normal stiffness (k_n) and tangential stiffness (k_s),

$$\sigma = \sigma_0 + k_n \Delta u_n \tag{5}$$

$$\tau = \tau_0 + k_s \Delta u_s \tag{6}$$

where σ and σ_0 are the normal stress of the sub-contact in the current and in the previous iteration, respectively; τ and τ_0 are the tangential stress of the sub-contact in the current and in the previous iteration, respectively.

The stresses determined by equations (5) and (6) have to be checked against the joint constitutive model adopted, which is the Mohr-Coulomb failure criterion. Different contact integration procedures for the stress diagram can be adopted and six solutions have been implemented: point model (pt), rectangular model with two control points (r2pt), rectangular model with three control points (r3pt), trapezoidal model with two control points (t2pt), trapezoidal model with three points control (t3pt) and trapezoidal model with moving control points (tptm). The control points are the points where the stresses are checked in terms of the constitutive model. For models with two control points, these points correspond to sub-contacts 1 and 2, whose stresses are determined by equations (5) and (6). In models with three points, the third point corresponds to the midpoint of the contact, whose stress is determined taking into account a linear distribution of stresses. In the model of moving points, the points are introduced in

places where violations of the constitutive model are detected. In this model the number of control points is not predefined, being introduced for the correct definition of the final diagram. Figure 6 shows a comparative study of the contact models. Four mesh sizes were used to study the convergence of the results, and the present model formulations were also compared with a well-known commercial software based on the discrete element method, namely UDEC [5]. The graphic represents the vertical stress at the toe of the dam, for various discretization levels, due to the self-weight of the dam and the hydrostatic pressure. The height and base of the dam are 100 and 80 m respectively, while the reservoir height is 100 m. The properties of the material of the dam body are 30 GPa for the Young's modulus, 0.2 for Poisson's ratio and the density is 2400 kg/m^3. The dam is laid out on a rigid block, whose movements are restricted in both horizontal and vertical directions. An elastic joint is adopted in the dam-foundation interface, with a normal stiffness of 30 GPa/m and a tangential stiffness of 10 GPa/m. For 16 elements at the base, the tptm contact model converged to a final stress value, while the other contact models did not yet reach it.

In the point contact model (pt), after integration, the forces are distributed directly at the sub-contact application point, so the resultants forces are not statically compatible with the diagram that originated them, even if this model is the one most commonly used in DEM codes. As expected, the stresses obtained with UDEC are equivalent to the pt contact model. In the model of rectangular contact with two control points, the integration is done in the same way, but the resultant forces are applied to the middle of the influence area of each sub-contact and from these points are allocated to the sub-contacts application points, yielding a set of forces statically consistent with the diagram of stresses. The same observation applies to the rectangular model with three control

points. In this case, the diagram is discretized using three rectangles, unlike the previous models, which use only two rectangles.

All models that use trapezoidal diagrams of stresses give rise to forces which are distributed through the sub-contacts application points in a way statically compatible with the diagram of stresses. In the case of the model with three control points, the diagram is approximated by two trapezoidal stress diagrams, which share one side. In the model with moving points, the stress diagram is decomposed by trapezoids, as many as necessary to define the diagram and, subsequently, the forces are distributed through the sub-contacts application points. Figure 7 shows the constitutive model test for normal direction, for both elastic behaviour and in case of violation of the tension and compression limits, shows the integration of the stress diagram and shows the distribution of the resultant forces for *pt* contact model and *tptm* contact model.

The method of integration controls the rotation stiffness of the contact. The point model is the most rigid, while trapezoidal models are more flexible, presenting all the same rotation stiffness in case of linear elastic analysis. The model of moving points is the one with the more accurate integration scheme and should be adopted in parts of the model where stress analysis is important. In parts of the model not directly involved in the failure mechanism being assessed, the point model can be used, as it is more robust and requires less computation time [18].

3. Integration of the equations of motion

Numerically, the incremental step involves setting up and integrating the equation of motion for each degree of freedom of the model,

$$c\dot{u} + m\ddot{u} = f_{TOT} \tag{7}$$

$$f_{TOT} = f_{EXT} + f_{INT} + f_{CT} + f_M \tag{8}$$

where $\dot{u}$ is the velocity; $\ddot{u}$ is the acceleration; c is the viscous damping coefficient; m is the mass; f_{TOT} is the total force; f_{EXT} is the external force; f_{INT} is the internal force, equivalent to the stress field of the element (only for deformable blocks); f_{CT} is the contact force; and f_M is the mass force. Damping includes only the component proportional to the mass,

$$c = \alpha m \tag{9}$$

where α is the viscous damping coefficient. The internal forces are calculated according to standard FEM practice [19],

$$f_{INT} = \int_A B^T \sigma dA \tag{10}$$

where B^T is the transposed matrix of deformation; σ is the stress field; and A is the area of the element. Blocks are typically assumed elastic, but other constitutive models for the block material can be used. The integration of the general equation of motion, which is a second order differential equation, is made explicitly, according to the method of the central difference. This method allows the velocity determination at intermediate instant $t + \Delta t/2$ from the velocity at instant $t - \Delta t/2$,

$$\dot{u}_{t+\Delta t/2} = \left(\dot{u}_{t-\Delta t/2} d_1 + \frac{f_{TOT}}{m} \Delta t \right) d_2 \tag{11}$$

$$d_1 = 1 - \frac{\alpha \Delta t}{2} \tag{12}$$

$$d_2 = \frac{1}{1+\frac{\alpha \Delta t}{2}} \tag{13}$$

In linear deformable blocks, involving four corners, there are a total of eight degrees of freedom corresponding to two translations for each vertex, one in the horizontal direction (*x*) and the other in the vertical direction (*y*). Rigid blocks have only three degrees of freedom, independently of the number of vertices of the block. These three degrees of freedom refer to the centroid of the block and correspond to the two translations and one rotation. The rotation is obtained from the angular velocity of the block determined by the following first order differential equation,

$$\alpha I \omega + I \dot{\omega} = M_{TOT} \tag{14}$$

$$M_{TOT} = M_{EXT} + M_{CTO} \tag{15}$$

where ω is the angular velocity; $\dot{\omega}$ is the angular acceleration; I is the moment of inertia; M_{TOT} is the total moment; M_{EXT} is the moment from external forces; M_{CTO} is the moment from contact forces.

The integration of equation (14) follows the procedures described for integration of equation (7). The velocity in the intermediate instant $t + \Delta t/2$ is given by,

$$\omega_{t+\Delta t/2} = \left(\omega_{t-\Delta t/2} d_1 + \frac{M_{TOT}}{I} \Delta t \right) d_2 \tag{16}$$

The displacements are obtained in an incremental way, as,

$$u_{x,t+\Delta t/2} = u_{x,t-\Delta t/2} + \dot{u}_{x,t+\Delta t/2}\Delta t \tag{17}$$

$$u_{y,t+\Delta t/2} = u_{y,t-\Delta t/2} + \dot{u}_{y,t+\Delta t/2}\Delta t \tag{18}$$

where u_x is the total displacement in *x* direction; u_y the is the total displacement in *y* direction.

In each incremental step, the position of the vertices of a block is given by,

$$x_{t+\Delta t/2} = x_{t-\Delta t/2} + u_{x,t+\Delta t/2} \tag{19}$$

$$y_{t+\Delta t/2} = y_{t-\Delta t/2} + u_{y,t+\Delta t/2} \tag{20}$$

where x and y are the vertex coordinates.

For vertices of deformable blocks the linear velocities are obtained directly by equation (11). For the rigid blocks, the linear velocities are achieved by means of the linear velocity of block centroid and from the angular velocity of the block. In the latter case, for a specific vertex, the linear velocities are given by,

$$\dot{u}_x = \dot{u}_{x,CM} - \left(y - y_{CM}\right)\omega \tag{21}$$

$$\dot{u}_y = \dot{u}_{y,CM} + \left(x - x_{CM}\right)\omega \tag{22}$$

where x_{CM} and y_{CM} are the centroid coordinates of the block.

3.1. Time step determination

The process of explicit integration of the equation of motion, using the central difference method, imposes a numerical restriction on the value of the time step. The time step should be lower than the time required for a longitudinal wave to travel through the smallest elastic element in the model. According to the Courant criterion, the following equation should be observed [20],

$$\Delta t \leq \frac{L_{min}}{C_p} \tag{23}$$

where Δt is the time step; C_P is the propagation velocity of a longitudinal wave; and L_{min} is the minimum distance between two vertices or between a vertex and an edge. In an elastic system [20], this is equivalent to

$$\Delta t \leq \frac{2}{\omega} \tag{24}$$

where ω is the highest natural frequency.

An upper-bound of this frequency can be estimated from the mass and stiffness of each degree of freedom of the model. The time step will then be restricted by the following equation,

$$\Delta t \leq min\left(2\sqrt{\frac{m_i}{k_i}}\right) \tag{25}$$

where m_i is the mass of the degree of freedom *i*; and k_i is the stiffness associated with the degree of freedom *i*. For deformable blocks the masses are determined from the mass matrix,

$$M = \int_A \left(N^T \rho N \right) dA \tag{26}$$

where M is the mass matrix (8 × 8 or 6 × 6); N are the shape functions; and ρ is the density. This integral is solved by the Gauss method and, in the explicit algorithm adopted, it is necessary to diagonalize the matrix mass. For the degree of freedom *i*, the mass is the sum of the row of the mass matrix,

$$m_i = \sum_j M_{i,j} \tag{27}$$

The stiffness of each degree of freedom of the deformable block has a component due to the block ($k_{BL,i}$) and another due to the contacts ($k_{CT,i}$). The component due to the block is determined by the stiffness matrix of the element, from the sum of the row corresponding to the degree of freedom (Gershgorin theorem),

$$k_{BL,i} = \sum_j \left| K_{i,j} \right| \tag{28}$$

where K is the stiffness matrix (8 × 8 or 6 × 6).

As the contact is established between the edges of the blocks, for the degrees of freedom associated with the vertices of these edges, the stiffness is estimated for each contact, as follows,

$$k_{CT,i} = \sum \left(k_n + k_s \right) L_i \tag{29}$$

where k_n and k_s are the normal and tangential stiffnesses; and L_i is the influence length.

In rigid blocks, the time step can be dependent upon the stiffness of rotation and it is necessary to determine also the moment of inertia,

$$I = \sum_i m_i D_i^2 \tag{30}$$

where I is the moment of inertia at the centroid; and D_i is the distance to the degree of freedom *i*. The stiffness of rotation (k_{ROT}) is obtained by analogy with the moment of inertia,

$$k_{ROT} = \sum_i k_{CT,i} D_i^2 \tag{31}$$

The time step should be lower than,

$$\Delta t \leq min\left(2\sqrt{\frac{I}{k_{ROT}}}\right) \tag{32}$$

3.2. Scaled mass for static analysis

For static calculations, the aim is to examine the conditions under which the final state of equilibrium is reached. The transient phase, which corresponds only to the numerical convergence of the model, can thus be neglected. For this reason, the scaled mass technique is used to obtain maximum computational efficiency.

For deformable blocks, the scaled mass for the degree of freedom *i*, is given by,

$$m_{SC,i} = \frac{\Delta t^2}{4}\left(k_{BL,i} + k_{CT,i}\right) \tag{33}$$

where $m_{SC,i}$ is the scaled mass of the degree of freedom *i*.

In rigid blocks it is necessary to scale the mass of the degrees of freedom with respect to the centroid, in particular the mass in the directions *x* and *y*, using the equation (33), and the moment of inertia,

$$I_{SC} = \frac{\Delta t^2}{4} k_{ROT} \tag{34}$$

3.3. Dynamic relaxation

The static solutions are obtained by a process of dynamic relaxation, using scaled masses and artificial damping. Viscous mass-proportional damping is used, with an adaptive scheme that updates the damping coefficient step-by-step based on the dominant frequency of the structure from the Rayleigh quotient [21]. To determine the Rayleigh quotient, it is necessary to calculate the tangent stiffness for each degree of freedom, $k_{TAN,x}$ and $k_{TAN,y}$,

$$k_{TAN,x} = \sum \left[\frac{\left(f_{INT,x,t+\frac{\Delta t}{2}} - f_{CT,x,t+\frac{\Delta t}{2}} \right) - \left(f_{INT,x,t-\frac{\Delta t}{2}} - f_{CT,x,t-\frac{\Delta t}{2}} \right)}{\dot{u}_{x,t-\frac{\Delta t}{2}} \Delta t} \right] \tag{35}$$

$$k_{TAN,y} = \sum \left[\frac{\left(f_{INT,y,t+\frac{\Delta t}{2}} - f_{SCT,y,t+\frac{\Delta t}{2}} \right) - \left(f_{INT,y,t-\frac{\Delta t}{2}} - f_{SCT,y,t-\frac{\Delta t}{2}} \right)}{\dot{u}_{y,t-\frac{\Delta t}{2}} \Delta t} \right] \tag{36}$$

Thereafter the Rayleigh quotient, Q_{RAY}, is calculated for the model,

$$Q_{RAY} = \frac{\sum_n \left[k_{TAN,x} \left(\Delta u_x \right)^2 + k_{TAN,y} \left(\Delta u_y \right)^2 \right]}{\sum_n \left[m_x \left(\Delta u_x \right)^2 + m_y \left(\Delta u_y \right)^2 \right]} \tag{37}$$

The mass-proportional damping is given by,

$$\alpha = 2\sqrt{Q_{RAY}} \tag{38}$$

Numerical models of dams might have parts with different dynamic behaviour, namely the dam and foundation. It is therefore possible to select the blocks that will contribute to determining the overall coefficient. This calculation scheme also allows a reduction in processing time. The adaptive scheme described was found to provide a smoother convergence path than other dissipation options, such as the non-viscous local damping [18].

4. Application case study

The Guilhofrei Dam (Figure 8) is located in the municipality of Vieira do Minho, northern of Portugal. This is a masonry gravity dam, designed by A. Stucky and completed in 1938. The dam has a maximum height of 39 m above the foundation, with a total length of 190 m, measured at the crest. The dam has a set of six vertical joints, which divide the structure into seven blocks. Without taking into account the central block, which has a higher penetration in the foundation, the block located between the joints D and E, block DE (Figure 9), the third from the left margin, has the highest height (about 30.6 m) and is likely to determine structural safety. The dam is built on a granitic rock mass, formed by coarse- to medium-grained biotite granites, generally of

good quality. The foundation (Figure 10a) has a slope of 10% and, at the heel, there is a shear-key with a length of 3 m.

The following analyses were carried out: (i) analysis of stresses in the dam and in the dam-foundation interface for the action of the self-weight (SW), the hydrostatic pressure (HP) and the self-weight and the hydrostatic pressure (SW+HP); (ii) analysis of safety against local failure of the dam material for the action of SW+HP; (iii) analysis of the safety against local failure of the dam body considering a scenario of cohesion loss of the masonry; and (iv) sliding safety verification for different failure planes, for the SW+HP with uplift (U) (SW+HP+U) and for the flood scenario. The model used in the analyses (i), (ii) and (iv), is shown in Figure 10. As the dam-foundation interface was the critical safety concern, it was possible to simplify the model, adopting an equivalent continuum media for both dam and foundation, except for the analysis (iii). Therefore, in the other cases, only the dam-foundation interface was assumed to have a non-linear behaviour. For all analyses, the tptm contact model is adopted, using a "variable connectivity" approach. The detection of new contacts and the verification of existing contacts are carried out using a tolerance of 5mm.

4.1. Analysis of stresses in the dam and on the dam-foundation interface

The properties of the materials of the dam and foundation were 10 GPa for the Young's modulus and 0.2 for Poisson's ratio. Densities were 2400 kg/m^3 for the dam and 2500 kg/m^3 for the foundation. The elastic properties of the dam-foundation interface were 10 GPa/m for the normal stiffness and 3.0 GPa/m for shear stiffness. They are consistent with other numerical analyses of masonry gravity dams [18]. The total self-weight of the section is approximately 9700 kN/m. The horizontal component of the hydrostatic

pressure, upstream-downstream direction is approximately 5000 kN/m, while the vertical component, crest-foundation direction, corresponds to approximately 5% of the horizontal component. The support conditions were imposed on the rock mass model to prevent its translation in both directions: horizontal restrictions on the vertical external faces and vertical restrictions on the base of the model.

For the principal stress field due to the action of self-weight, the model does not present tensile stresses, being 0.94 MPa the maximum compression reached near the upstream heel. The self-weight action, assumed to be applied in one step, gives rise to a displacement field, whose maximum horizontal displacement near to the crest, in upstream direction, is about 2.5 mm. For the stress field due to the action of hydrostatic pressure, the maximum tensile stress is located at the heel, with a maximum value of 0.84 MPa. The maximum compressive stress occurs at the toe and reaches about 0.77 MPa. The maximum displacement occurs along the crest, upstream-downstream direction, with a maximum of 6.5mm. The bending component may in fact be lower, because the analysis does not take into account the 3D effects. Figure 11a represents the principal stress field at the elements gravity center generated by the action of the self-weight and hydrostatic pressure considering non-linear behaviour. There are no tensile stress and compressions are located downstream along the toe, with a maximum value of 0.96 MPa. The displacement field (Figure 11b) exhibits a maximum horizontal displacement, upstream-downstream, of 4 mm.

Stresses along the dam-foundation interface were obtained from the numerical contacts between the dam and the foundation. The stresses obtained with DEM were compared with diagrams assuming a linear distribution, as done in the limit equilibrium method (LEM), obtained from CADAM [22]. The vertical stresses due to the action of the self-

weight and hydrostatic pressure are shown in Figure 12. Note the very good agreement between LEM and DEM, with the exception of the peaks at the edges due to the discretization and elastic singularities. Those conclusions are consistent with others studies [23].

4.2. Local failure safety analysis

The analysis of the local failure of the continuum material is made based on the Mohr-Coulomb criterion, with a tensile and compressive cut-off. For each point, the safety factor will be the lowest among the failure in tension, compression and shear stress. For the first two cases, failure in tension for a tensile strength f_t and failure in compression for a compressive strength f_c, the safety factor is obtained by, respectively,

$$FS_{RL,t} = \frac{f_t}{\sigma_1} \tag{39}$$

$$FS_{RL,c} = \frac{f_c}{|\sigma_2|} \tag{40}$$

where $FS_{RL,t}$ and $FS_{RL,c}$ are local failure safety factors; σ_1 is the maximum tensile stress; σ_2 is the maximum compressive stress.

The failure by shear stress occurs in the direction of the point where Mohr's circle does not respect the envelope defined by the material properties. The safety factor is given by the ratio between the radius of the Mohr's circle which characterizes the stress state of the point and the radius of the critical Mohr's circle obtained by extrapolation of original Mohr's circle. The radius is achieved by increasing the shear stress, keeping constant the normal stress,

$$FS_{RL,s} = \frac{R_2}{R_1} = \frac{c\cos\phi + |\sigma_m|\sin\phi}{R_1} \tag{41}$$

where $FS_{RL,s}$ is a local failure safety factor; R_1 is the radius of the initial Mohr's circle; R_2 is the radius of the critical Mohr's circle; and σ_m is the normal stress.

This analysis is based on the results obtained for the state of stress due to the action of self-weight together with the hydrostatic pressure (Figure 11a). The section was analysed according to three different material property scenarios, given the uncertainty regarding the dam material. For these three situations, a friction angle of 55° and a compressive strength of 10 MPa have been adopted. For the first case, the tensile strength is 1.0 MPa and the cohesion is 1.58 MPa. In the second case the tensile strength is 0.5 MPa and cohesion is 1.12 MPa. In the third case, the less favourable, a tensile strength of 0.25 MPa and the cohesion is 0.79 MPa are assumed. According to Figure 13, the shear failure criterion is dominant for almost the entire section. The safety factors (FS_{RL}) obtained are higher than those recommended by the Portuguese regulation [24] (FS > 2.5), except locally, for intermediate and low properties, which led to safety factors, at the toe, of 2.3 and 1.9. Those peak values are obtained near the interface between the dam and the foundation, which are influenced by the model discretization on this region.

4.3. Local failure of the dam body considering a scenario of loss cohesion of the masonry

For the safety analysis of masonry dams, the degradation of the mortar and the consequent cohesion loss of the material is an imperative scenario to consider. In the case of Guilhofrei Dam, it is advisable to check this hypothetical scenario and to

investigate failure mechanisms in the dam body. Three models were developed with randomly generated Voronoi polygons (Figure 14), with an average side of 2 meters length.The upstream and downstream faces were composed of quadrilateral elements.

The joints between the dam blocks were assigned an inelastic behaviour with null cohesion and tensile strength. The boundary conditions, restrictions on the vertical and horizontal movements, are imposed directly on the base of the dam, since the objective was the analysis of the failure in the dam body. Throughout the analysis, the friction angle was reduced, in steps of 0.5°, until the structure fails, i.e. the model does not converge to an equilibrium solution. In the first model (Model A), the failure takes place from a friction angle of 18°. The failure mechanism occurs at crest. The same happens with the second model (Model B) but, in that case, the friction angle is about 17°. The Model C fails in a different way, with more distributed cracks, showing higher resistance, with an angle of 15º. The differences of the Voronoi meshes dictate some variation in the results, but the main behaviour is similar in the three models, with failure taking place in the critical section at the elevation where the downstream face slope changes.

4.4. Safety assessment of the sliding failure scenario

Four analyses were performed for the sliding failure of the dam for different planes and different loads. The first analysis (S_1) evaluates the possibility of sliding along a plane of failure through the dam, without taking into account the effect of the upstream shear-key (Figure 15a). The analysis S_2 considers a plane that involves the failure of part of the foundation (Figure 15b). The analysis S_3 is similar to the analysis S_1, but the presence of the upstream shear-key was considered (Figure 15c). Finally, the analysis

S_4, also similar to the S_1 analysis, considers the possibility of the occurrence of a water level corresponding to a flood scenario.

For the first three analyses, the combination SW+HP+U is considered. The uplift is applied, with a reduction of 2/3 due to the drainage system located in the gallery at about 5 m from upstream. From the heel to the drainage gallery, the vertical component of uplift is 1015 kN/m and from the drainage gallery to the toe the vertical component of uplift is 975 kN/m. The horizontal component is not applied because its action would contribute to the safety of the dam.

For the analyses S_1 and S_2, after the application of the hydrostatic pressure and before the application of uplift, the properties of the dam-foundation interface are changed and the joint assumes an inelastic behaviour, with the tensile strength and cohesion assumed zero. The sliding scenario is assessed through a parametric analysis of the friction angle of the dam-foundation interface. The value of the friction angle is reduced successively until failure is reached, i.e. the model does not converge to an equilibrium solution. In the analysis S3, the change in properties of the dam-rock interface does not include the shear-key for which both tensile strength and cohesion are taken as 1.0 MPa, and the friction angle is 45°. The properties are reduced about 15% at each iterative step, until the structure collapses, with the reduction factor being applied to the entire failure plane, including all the properties of the shear-key. The results for the horizontal displacements of the crest as a function of the friction angle adopted, for the three analyses, are shown in Figure 16.

The analysis S_2 shows higher elastic displacement than analysis S_1, since the average inclination of the foundation plane is lower. Nevertheless, failure occurs for a friction angle slightly lower. This occurs because the friction area of the sliding surface in the

model S_2 is higher than in the model S_1. The sliding safety factor, for a nominal angle of 45°, is equal to 1.9 for model S_1 and 2.1 for model S_2. As expected, the model with shear-key (S_3) has a lower elastic displacement when compared with the model S_1 and the failure occurs for a lower friction angle. The model S_3 presents a safety factor of 2.4. The increase in safety due to the presence of the shear-key is about 26%.

Another sliding analysis was performed for the combination of SW+HP+U in association with the flood scenario (S_4). The action due to flooding is applied incrementally. In each step, the level of the reservoir rises 1 m, which increases the hydrostatic pressure and the uplift in equivalent parts. The uplift was added only in the section that begins at the heel and ends at the drainage gallery. The failure mechanism has a significant component of overturning. The results are shown in Figure 17. For each step, the crack length along the foundation, in the upstream zone which is under tensile stress, and the maximum compression stress, on downstream, were registered. The section, in this last analysis S_4, is stable for a reservoir level up to 5 m above the dam crest. Collapse is therefore unlikely, since in case of flood, the gates are open in advance and, if necessary, the bottom outlet and ducts of the production system can be used to increase the flow capacity. The failure mechanisms for S_1, S_2 and S_4 are shown in Figure 18.

5. Conclusions

A numerical model, based on the Discrete Element Method, is developed specifically for the analysis of masonry gravity dams and their foundations. The model and related code allow the stress analysis of the dam, as well as the analysis of the main failure mechanisms associated with masonry gravity dams, whether they involve the dam body,

the rock mass, or the dam-rock interface. The specific features of dams, and the needs required in their analysis, determined the adopted solutions for the numerical analysis tool, namely in terms of material and contact models, geometry and load data input, and processing of results.

The dam model is discretized into elementary blocks, which may be associated to form complex macroblocks. The interaction between macroblocks is represented by means of contacts between the elementary blocks. A formulation of face-to-face contact, more rigorous than the usual point contact assumption, was developed. The contact forces may be obtained from stresses according to different procedures, but the trapezoidal stress diagram was found to be the most appropriate. An explicit solution algorithm is used for both static and dynamic analysis. To improve computational efficiency, all the numerical aspects were implemented in an integrated manner. Accurate estimates of time steps and scaled masses are obtained using element stiffness matrices and contact stiffness, and an adaptive control of damping was implemented for dynamic relaxation.

The discretization options implemented provide great flexibility, allowing the application to simulate either an equivalent continuum or a truly blocky system. For dam safety analysis, simplified models concentrating on the behaviour of the dam-rock interface, or a few major discontinuities, have great practical interest, as in the example presented. Failure modes involving the rubble masonry in the dam may be analysed with regular patterns or with randomly generated blocks. An area for future development of the model is the representation of the inner structure of the masonry dam, for example, taking into account the often observed layering of blocks, but still including its typically irregular nature. Deformable blocks, corresponding to numerically integrated finite elements, provide the means for the indispensable stress

analysis in the dam body. Multiple failure modes can be assessed with minor changes in the numerical representation, which is an important issue in the analysis of existing masonry dams given the uncertainties regarding the present state of the material and the foundation conditions.

Acknowledgement

Permission by EDP to present the example data is gratefully acknowledged. The first author also acknowledges the financial support of the Portuguese Science Foundation (Fundação de Ciência e Tecnologia, FCT), through grant SFRH/BD/43585/2008.

References

[1] P.A. Cundall, A computer model for simulating progressive large scale movements in blocky rock systems, Rock Fracture (ISRM), Nancy, 1971.

[2] R.E. Goodman, R.L. Taylor, T.L. Brekke, A model for the mechanics of jointed rock, J. Soil Mech. Found. Div. ASCE 94(3): 637-659, 1968.

[3] W. Wittke, Rock mechanics. Theory and applications with case histories. Springer-Verlag, Berlin, 1990.

[4] P.B. Lourenço, Computations of historical masonry constructions, Progress in Structural Engineering and Materials 4 (2002) 301-319.

[5] Itasca, Universal Distinct Element Code (UDEC) – Version 5.0, Minneapolis, 2011.

[6] J.V. Lemos, Discrete element analysis of dam foundations, Distinct Element Modelling in Geomechanics, Eds. V.M. Sharma, K.R. Saxena, R.D. Woods, Balkema, Rotterdam, 1999, pp. 89-115.

[7] G. Barla, M. Bonini, G. Cammarata, Stress and seepage analyses for a gravity dam on a jointed granitic rock mass, 1st International UDEC/3DEC Symposium, Bochum, 2004, pp. 263-268.

[8] E. Gimenes, G. Fernández, Hydromechanical analysis of flow behavior in concrete gravity dam foundations, Canadian Geotechnical Journal 43(3): 244-259, 2006.

[9] B.S.A. Tatone, A. Lisjak, O.K. Mahabadi, G. Grasselli, C.R. Donnelly, A preliminary evaluation of the combined finite element-discrete element method as a tool to assess gravity dam stability, CDA Annual Conference, Niagara Falls, 2010.

[10] N. Petrinic, Aspects of discrete element modelling involving facet-to-face contact detection and interaction, PhD Thesis, University of Wales, Cardiff, 1996.

[11] E.M. Bretas, J.V. Lemos, P.B. Lourenço, Hydromechanical analysis of masonry gravity dams and their foundations, Rock Mech Rock Eng, 2012.

[12] FERC (Federal Energy Regulatory Commission), Engineering guidelines for evaluation of hydropower projects - Chapter III Gravity Dams. Federal Energy Regulatory Commission, Office of Hydropower Licensing, Report No. FERC 0119-2, Washington D.C., USA, 1991.

[13] USACE (US Army Corps of Engineers), Engineering and design: Gravity dam design. Report EM 1110-2-2000, Washington, D.C., 1995.

[14] USBR (United States Bureau of Reclamation), Design of small dams. Denver, Colorado, 1987.

[15] P.A. Cundall, Formulation of a three-dimensional distinct element model – Part I. A scheme to detect and represent contacts in a system composed of many polyhedral blocks, Int. J. Rock Mech. Min. Sci. & Geomech. Abstr. 25(3): 107-116, 1988.

[16] J.R. Williams, R. O'Connor, Discrete element simulation and the contact problem, Archives of Computational Methods in Engineering 6(4): 279-304, 1999.

[17] A. Munjiza, The combined finite-discrete element method, Wiley, West Sussex, 2004.

[18] E.M. Bretas, Development of a discrete element model for masonry gravity dams analysis, PhD Thesis (in Portuguese), Engineering School, University of Minho, 2012. Available from www.civil.uminho.pt/masonry.

[19] T.J.R. Hughes, The finite element method, Dover Publications, Inc., Mineola, 1987.

[20] T. Belytschko, An overview of semi discretization and time integration procedures, Computational methods for transient analysis, Elsevier Science Publishers B.V., Amsterdam, 1983, pp. 1-65.

[21] R.G. Sauvé, D.R. Metzger, Advances in dynamic relaxation techniques for nonlinear finite element analysis, Journal of Pressure Vessel Technology 117(2): 170-176, 1995.

[22] M. Leclerc, P. Leger, R. Tinawi, Computer Aided Stability Analysis of Gravity Dams - CADAM. Advances in Engineering Software, 34(7): 403-420, 2003.

[23] E.M. Bretas, J.V. Lemos, P.B. Lourenço, Masonry dams: Analysis of the historical profiles of Sazilly, Delocre and Rankine, International Journal of Architectural Heritage, 6(1): 19-45, 2012.

[24] NPB, Guidelines for design of dams (in Portuguese). Portaria N.º 846/93. Diário da República, Lisbon, 1993.

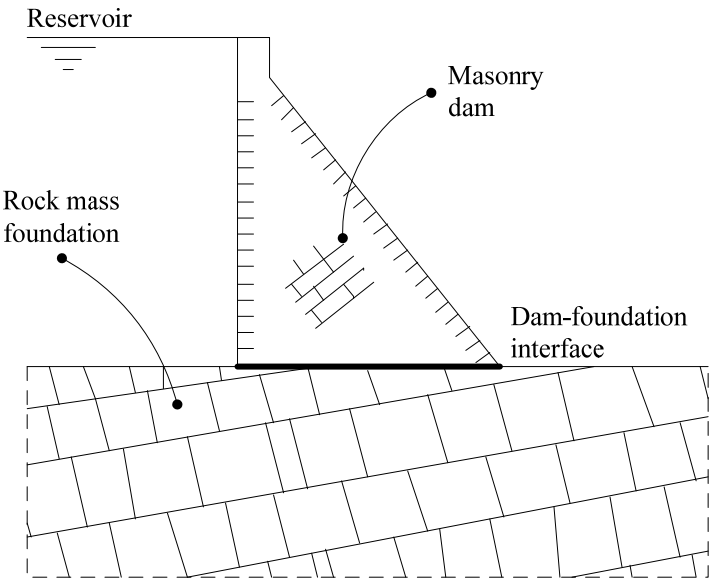

Figure 1 – Masonry dam and rock mass foundation forming discontinuous media

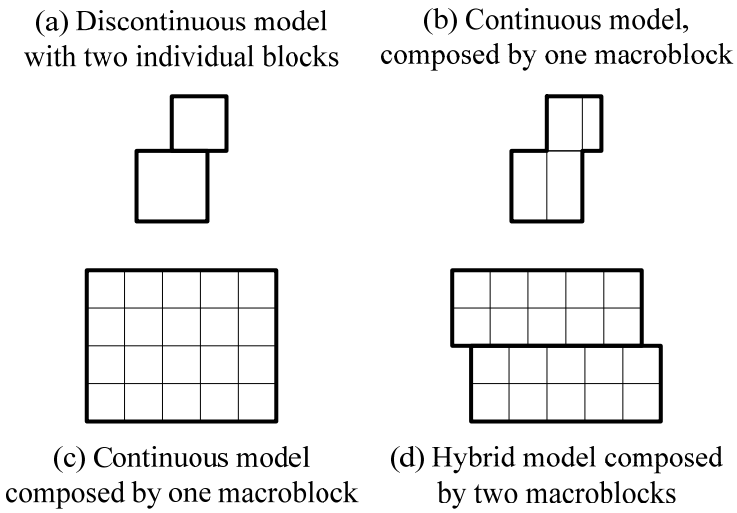

Figure 2 – Continuous and discontinuous models composed by macroblocks

(a) Contacts face-to-face type 1 (FF_1)

(b) Contacts face-to-face type 1 (FF_2)

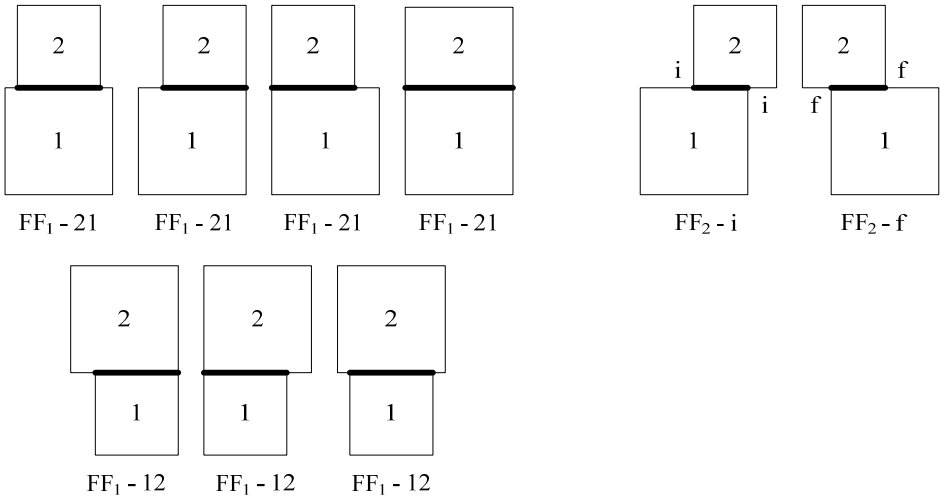

Figure 3 – Contacts face-to-face type 1 (FF_1) and contacts face-to-face type 2 (FF_2)

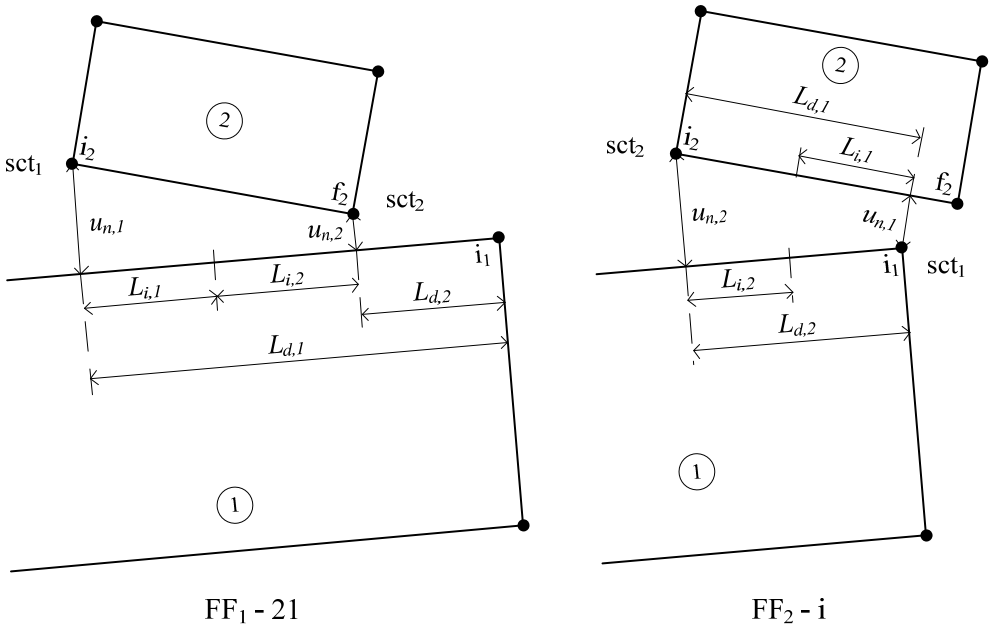

FF$_1$ - 21 FF$_2$ - i

Figure 4 – Data structure of the contacts type FF$_1$ (21) and FF$_2$ (i)

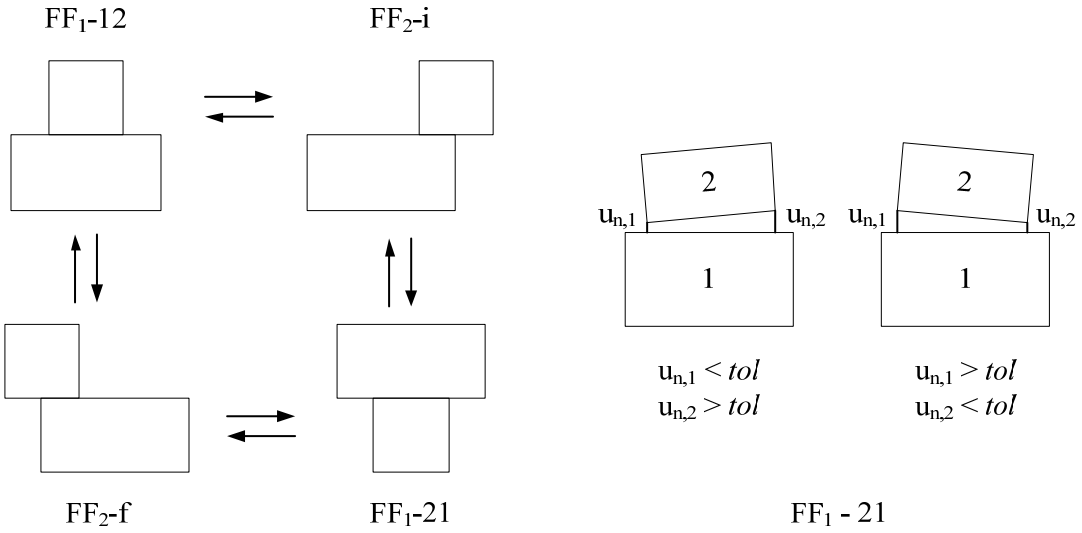

(a) Contacts reclassification (b) Contacts degeneration

Figure 5 – Contacts reclassification (a) and degeneration of face-to-face to vertex-to-face contact (b)

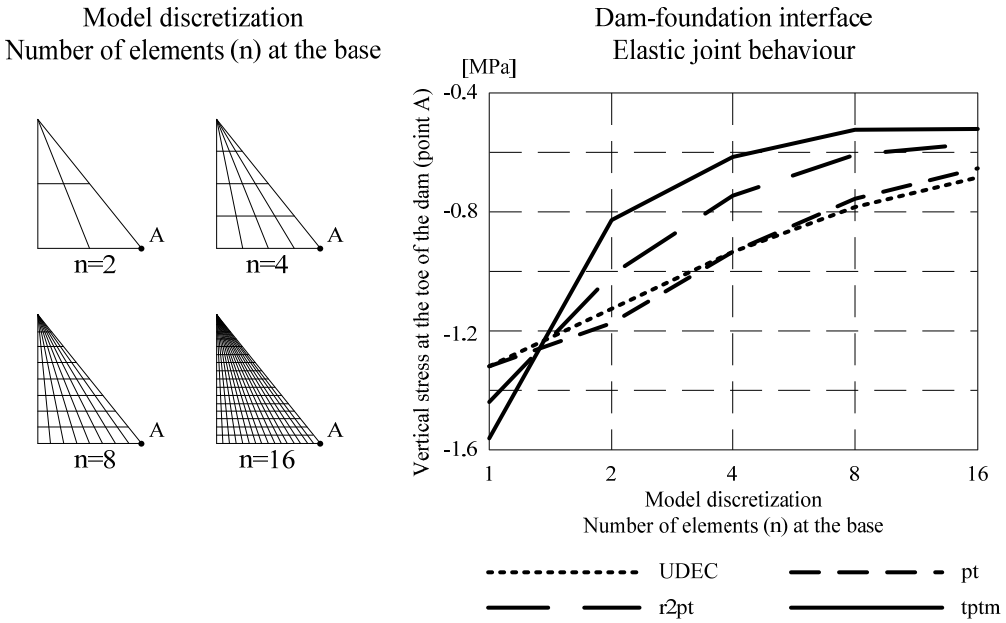

Figure 6 – Influence of contact integration scheme and model discretization for a dam subject to its self-weight and hydrostatic pressure

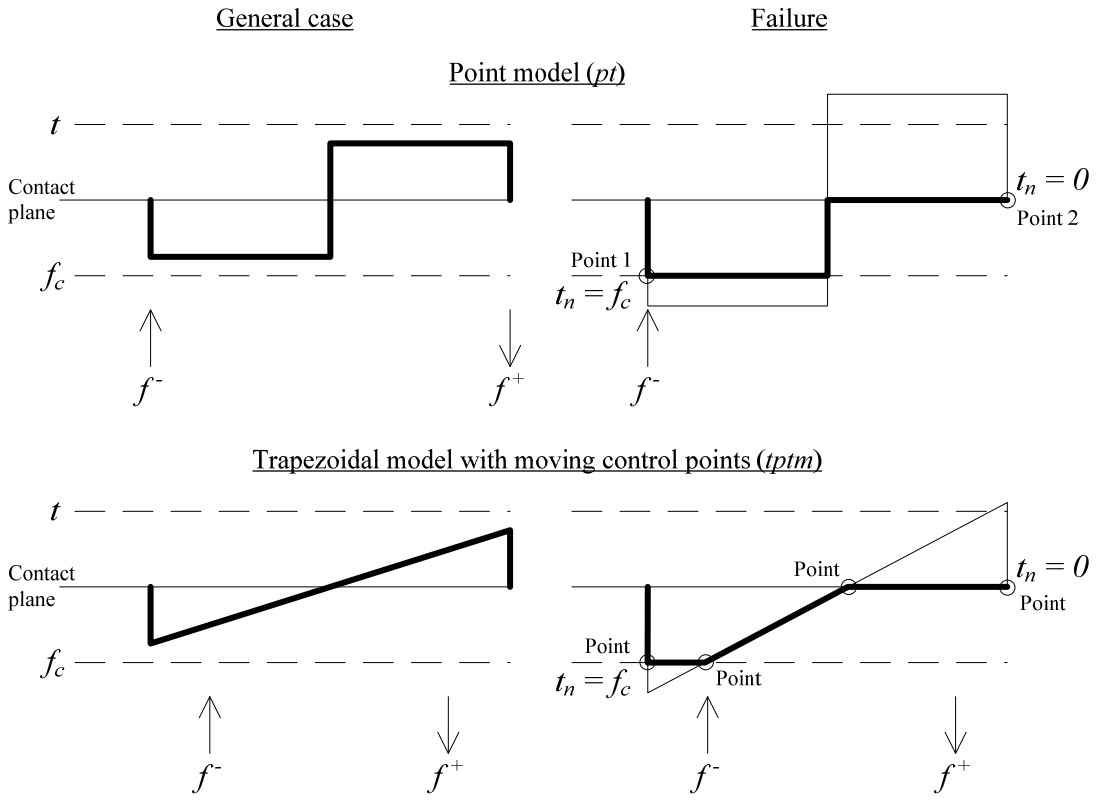

Figure 7 – Integration of the stress diagram and distribution of the resultant forces for *pt* contact model and *tptm* contact model

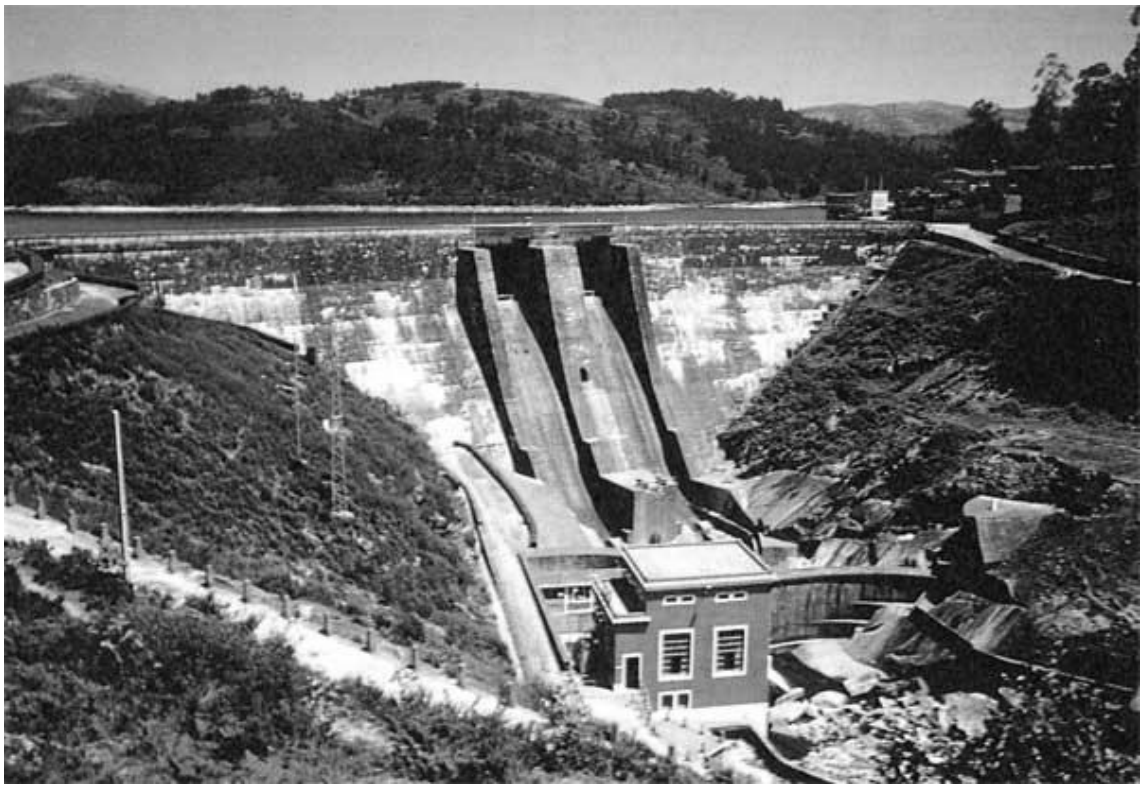

Figure 8 – View of Guilhofrei Dam from the downstream side

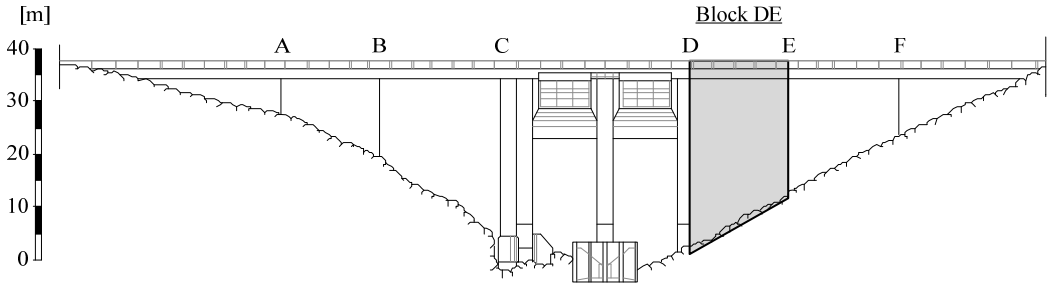

Figure 9 – View of the downstream face of the Guilhofrei Dam, identification of the block DE

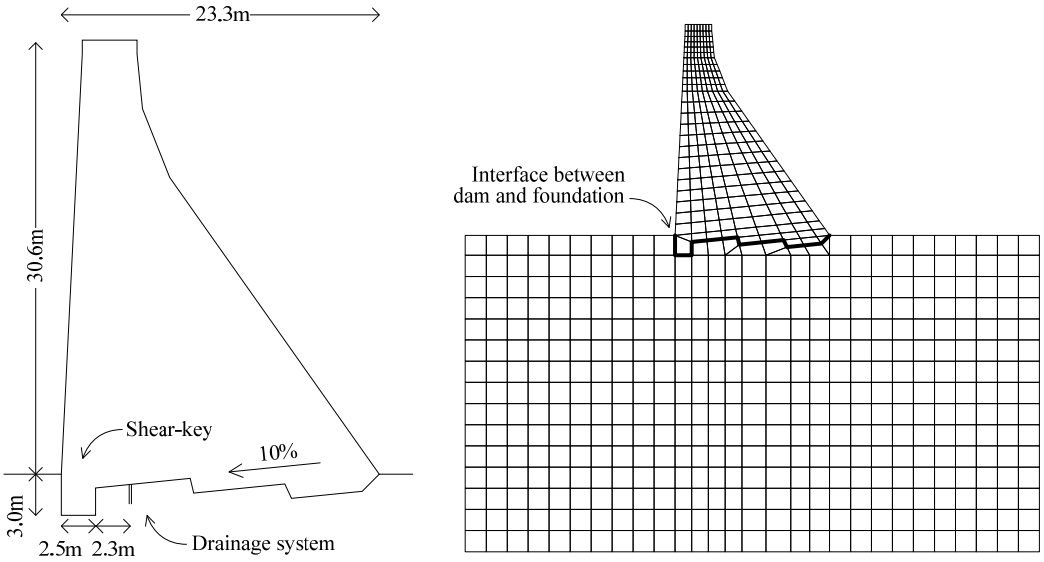

(a) Mid section of the block DE (b) Geometry and Discretization of the model

Figure 10 – Mid section of the block DE (a) and geometry and discretization of the model (b)

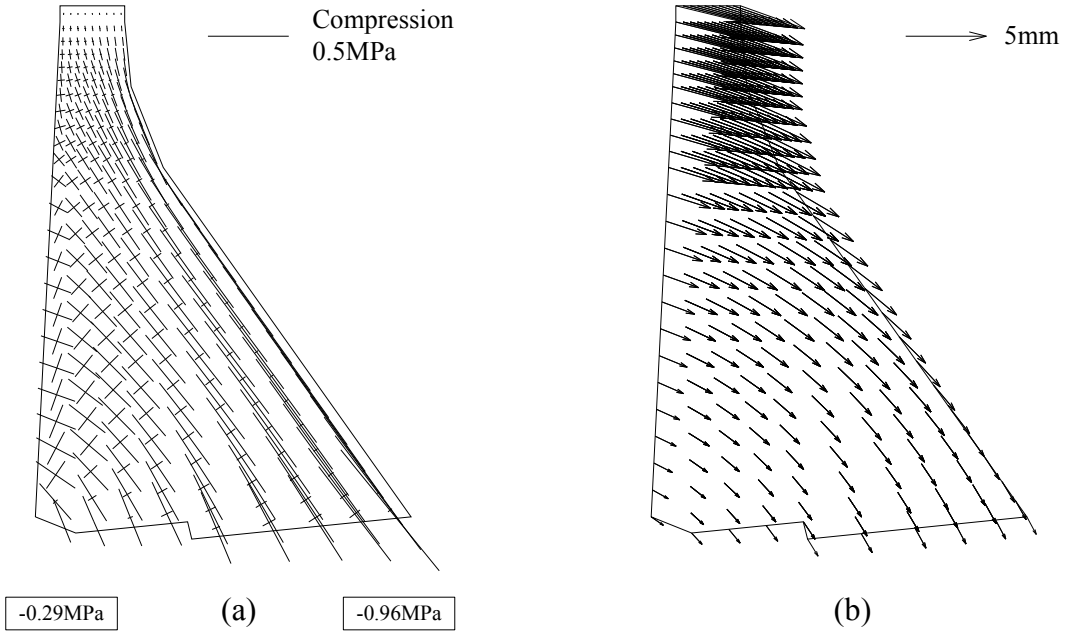

Figure 11 –Principal stress field at the elements gravity center (a) and displacement (b) due to action of the self-weight and the hydrostatic pressure (SW+HP)

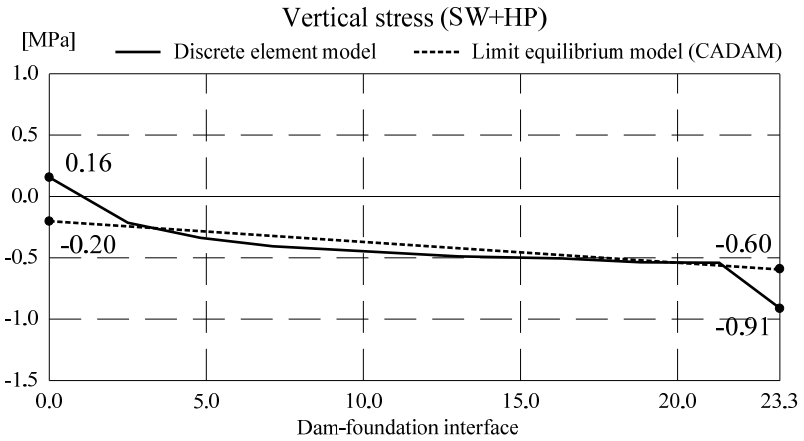

Figure 12 – Vertical stresses obtained from the discrete element model and from the limit equilibrium model (CADAM), due to action of the self-weight and the hydrostatic pressure (SW+HP)

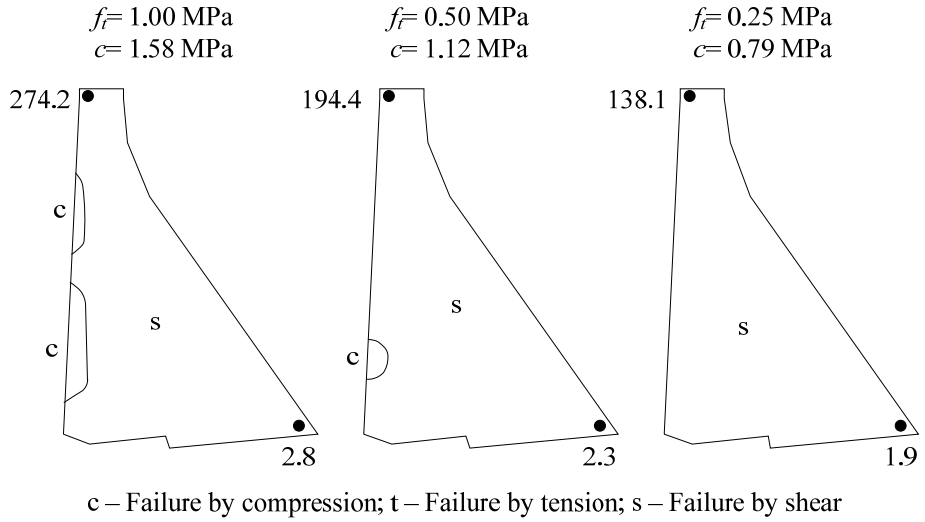

Figure 13 – Local failure safety factor (Mohr-Coulomb criterion), with local values at crest and toe.

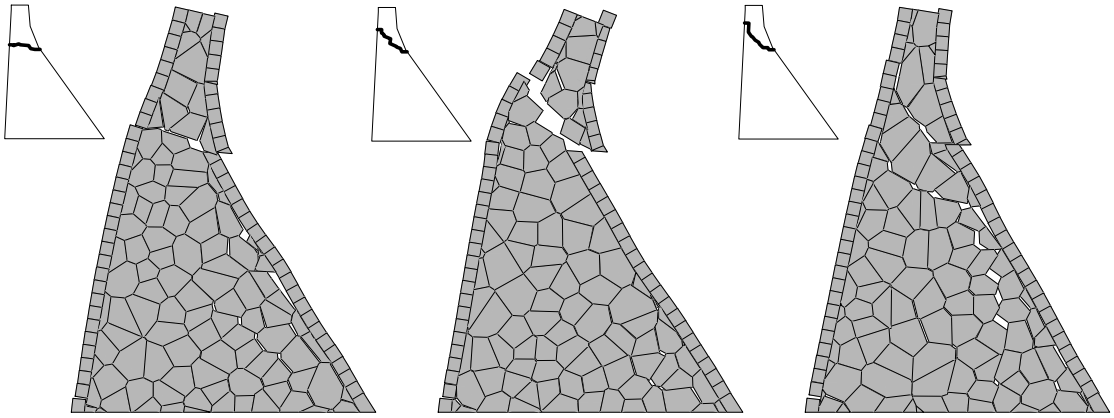

Figure 14 – Local failure observed on Voronoi models considering a loss of cohesion scenario (displacements are magnified)

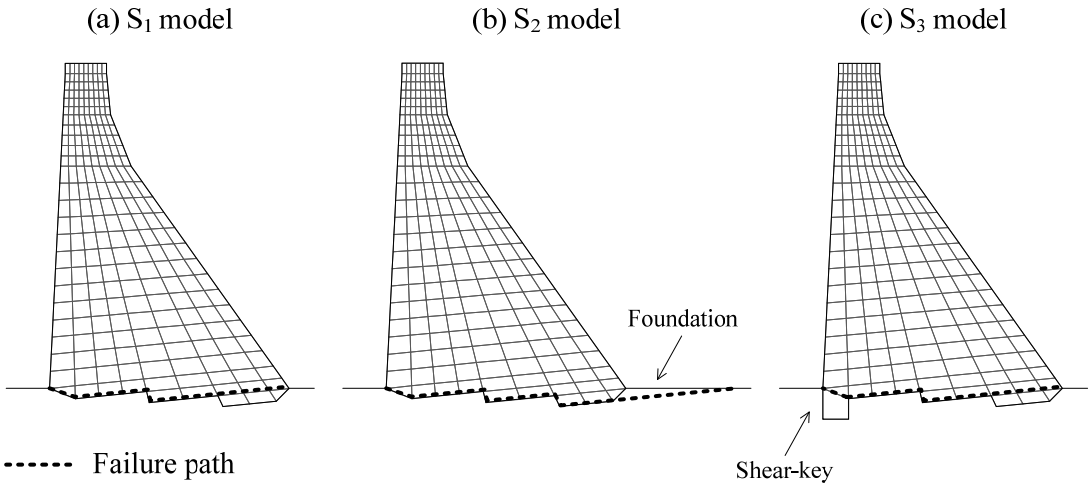

Figure 15 – Detail of failure path of the models S1, S2 and S3

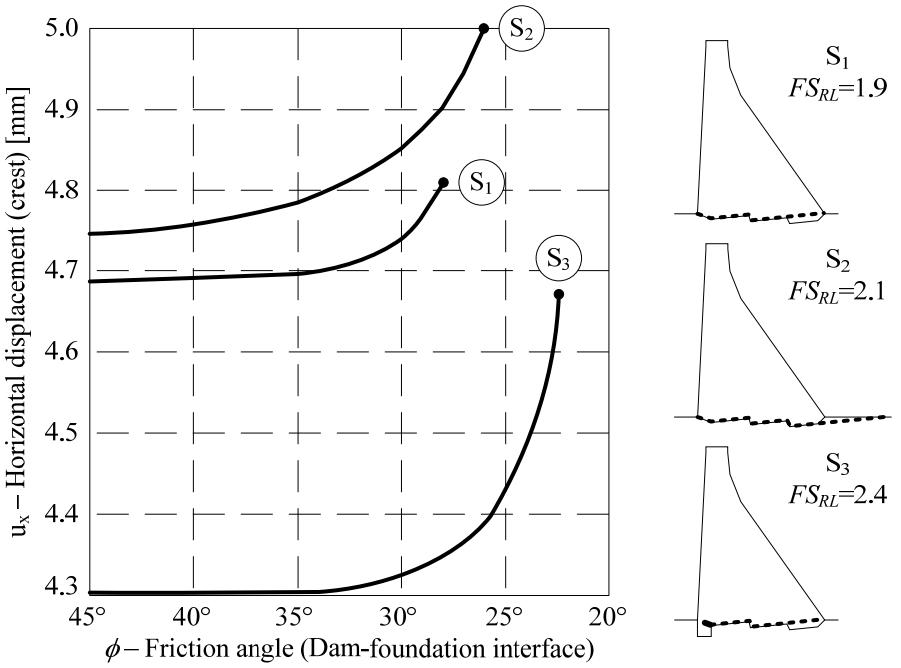

Figure 16 – Sliding analysis of the models S_1, S_2 and S_3

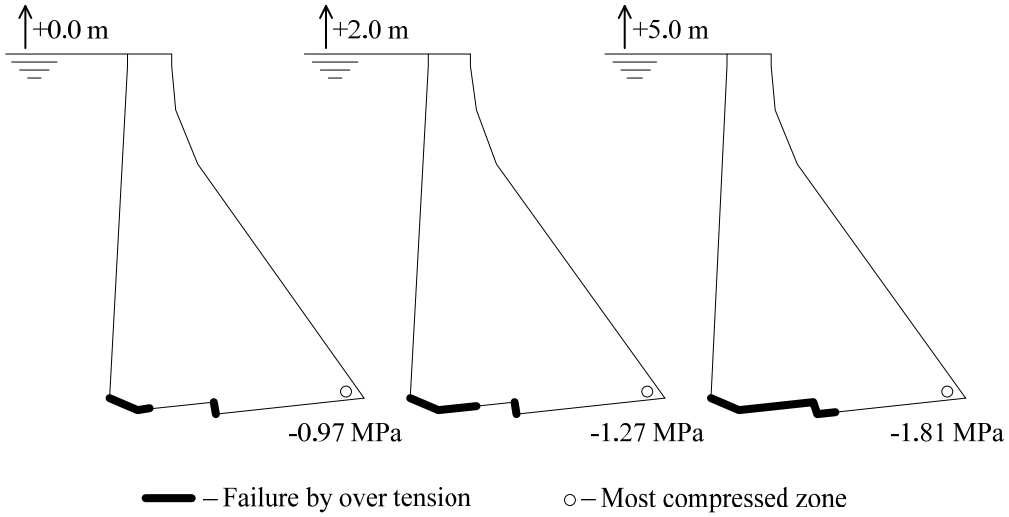

Figure 17 – Sliding analysis of the dam to a flood scenario (S_4), for levels +0.0 m, +2.0 m and +5.0 m

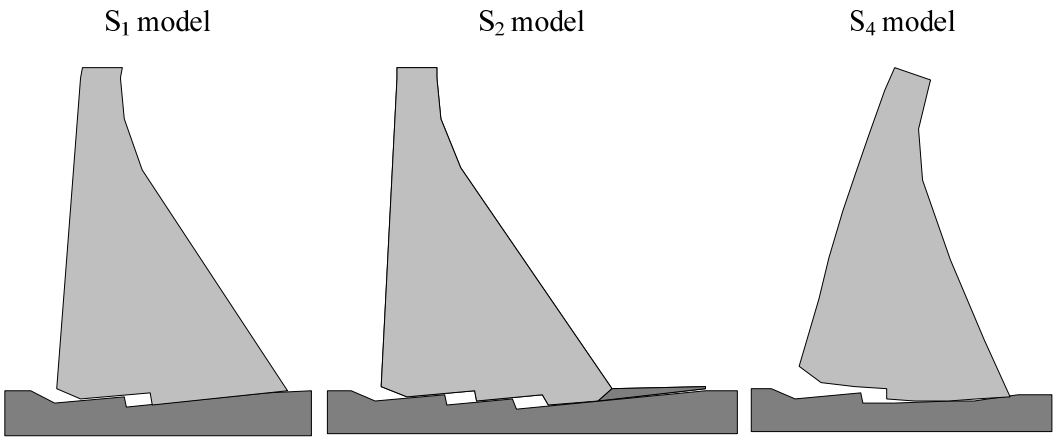

Figure 18 – Failure mechanism of the analyses S_1, S_2 and S_4 (displacements are magnified)